

Article

Strong Interrelation between the Short-Term Variability in the Ionosphere, Upper Mesosphere, and Winter Polar Stratosphere

Anna Yasyukevich ^{1,*}, Irina Medvedeva ¹, Vera Sivtseva ², Marina Chernigovskaya ¹, Petr Ammosov ² and Galina Gavrilyeva ²

¹ Institute of Solar-Terrestrial Physics SB RAS (ISTP SB RAS), 126a Lermontov st., 664033 Irkutsk, Russia; ivmed@iszf.irk.ru (I.M.); cher@iszf.irk.ru (M.C.)

² Yu.G. Shafer Institute of Cosmophysical Research and Aeronomy SB RAS, 31 Lenin Ave., 677980 Yakutsk, Russia; verasivtseva@gmail.com (V.S.); p.p.ammosov@ikfia.ysn.ru (P.A.); gagavrilyeva@ikfia.ysn.ru (G.G.)

* Correspondence: annpol@iszf.irk.ru

Received: 15 April 2020; Accepted: 14 May 2020; Published: 16 May 2020



Abstract: We perform a joint analysis of short-period (up to several hours) variability in parameters of the ionosphere, the mesosphere, and the stratosphere at mid-latitude, subauroral, and high-latitude points for a long time interval. The study is based on the ionospheric total electron content (TEC) measurements and data on the OH rotational temperature at the mesopause height. We reveal similar seasonal variations in the dynamics of the short-term variability level, both in the ionosphere and the mesosphere. Maximum variability is observed during winter months and it exceeds the values in summer period up to 5–6 times. The revealed dynamics has no explicit relation to the levels of geomagnetic and solar activities. We suggest that the instabilities in the high-velocity stratospheric subauroral winter jet stream may be a source of the recorded variability seasonal variations in the ionosphere and the mesosphere. We propose a new index to estimate a short-term variability in the stratosphere. The index is shown to experience similar regular seasonal variations with a maximum during winter months. We show a clear correlation between the mesosphere/ionosphere variability indices values and the stratosphere disturbance index. The correlation is shown to be higher for the mesosphere variability index as compared with that in the ionosphere, and at the high-latitude point located closer to the jet stream. The obtained results indicate a strong interrelation between the short-period variability in the ionosphere, in the upper mesosphere, and in the subauroral stratosphere. The results contribute to elucidating the basic mechanisms for a vertical coupling between different atmospheric layers.

Keywords: stratosphere; mesosphere; mesopause; temperature; ionosphere; atmospheric-ionospheric coupling; wave disturbances; TEC; GPS

1. Introduction

The Earth upper atmosphere is the region subject to both solar plus magnetospheric forcing, and the effect from underlying shells of the neutral atmosphere. The determining factor in the thermodynamic regime of the upper atmosphere is helio-geomagnetic activity.

At the same time, investigations evidence that the cause for the observed ionosphere variations may be atmospheric waves of various spatial-temporal scales (acoustic, internal gravity (IGWs), tidal, and planetary), propagating from the lower and the middle atmosphere [1–3]. IGWs from the sources located in the lower atmosphere may penetrate (under certain conditions) onto high altitudes, thus causing wave disturbances in the parameters of the upper mesosphere, thermosphere, and, as

consequence, in the parameters of ionospheric plasma [1,4]. Thereby, IGWs originating in underlying layers contribute essentially to variations in the thermodynamic regime and in the composition of the upper atmosphere, thus providing vertical coupling of the atmospheric layers.

In the upper atmosphere, there may exist both small-scale IGWs with short periods and small wavelengths, and mid- and large-scale IGWs having the horizontal wavelength from several tens to several thousands of kilometers. The periods of these waves may vary from several minutes to almost 24 hrs [5]. In [6,7], the contribution to ionospheric disturbance of sources in the lower atmosphere was shown to be comparable (by magnitude) with geomagnetic activity. Based on the simulation results, Liu et al. [8] demonstrated that the meteorological driving may play a key role in day-to-day variability of the ionosphere. The comparison between the wave disturbance in the parameters of the neutral atmosphere and those of the ionosphere may provide the information on the processes stipulating the dynamic coupling between different atmospheric layers.

IGWs at the mesosphere/lower thermosphere (MLT) heights are observed by nightside airglow. Propagating through the hydroxyl (OH) emission layer at ~ 87 km, IGWs modulate the temperature and the emission intensity [9,10]. Recording the OH emission is now the most common method for IGW ground-based observation within the MLT region. From OH airglows, one determines IGW horizontal wavelengths, phase velocity, and periods [11–13], and observes the IGW activity for a long time [14–17]. During the Deep Propagating Gravity Wave Experiment (DEEPWAVE), Taylor et al. [18] observed IGW propagation from the middle stratosphere to the MLT region. The authors recorded the wave penetration at higher altitudes, at least, 10 km above the OH emission layer. IGW intensities in the mesopause region are shown to feature substantial seasonal, quasi-biennial and interannual variations that may vary at different altitudes [16]. According to the authors, such differences may be attributed to the changes in the strengths of IGW sources in the atmosphere at different altitudes and locations, as well as to the conditions of wave propagation in the atmosphere. Medvedeva and Ratovsky [19], based on the OH emission spectral observations, concluded that the seasonal variation in the mesosphere variability have a well-pronounced maximum in winter months.

IGWs manifest themselves in the ionosphere mostly as traveling ionospheric disturbances (TIDs). TIDs contribute significantly to ionospheric disturbance. Analyzing the database for the ionospheric F2-layer parameters, Araujo-Pradere et al. [20] revealed that, at high and middle latitudes, the ionospheric variability presented by the sample standard deviation of ionospheric characteristics has a clear seasonal trend. Under quiet geomagnetic conditions, the lowest variability was found in the summer hemisphere, the maximal being in winter, with the equinoxes between the two extremes. The authors also revealed a strong local time dependence, particularly at high latitudes, with the nighttime variability always stronger than that in the daytime. Altadil [21] showed that, at the midlatitude Ebro station, the largest F-region variability occurs during nighttime. Ratovsky et al. [22] also confirmed that the nighttime total relative variability obtained from digisonde data in Irkutsk had a clear seasonal behavior with the maximum in winter, minimum in summer, and with intermediate values at equinoxes.

Frissell et al. [23] studied the climatology of daytime mid-latitude medium-scale traveling ionospheric disturbances (MSTIDs) observed by the Blackstone Dual Auroral Radar Network (SuperDARN). They found that MSTIDs were observed primarily fall through spring. Frissell et al. [24] focused on winter daytime MSTIDs observed at high latitudes from four high-latitude and six mid-latitude SuperDARN radars in North America. Kotake et al. [25] analyzed the total electron content (TEC) data from several GPS receivers at mid-latitudes. The authors also noted that seasonal variation in the MSTID activity differed between daytime and nighttime with the highest daytime MSTID activity in winter at all the regions analyzed.

Medvedeva and Ratovsky [19] showed that the winter IGW variability above Irkutsk exceeds the summer one both for the ionospheric and atmospheric variabilities, but in the IGW case the winter/summer ratio for the ionospheric variability (~1.7) is noticeably larger than that for the atmospheric variability (~1.2).

Among the reasons for seasonal differences in the ionospheric IGW variability, the following factors are discussed: seasonal variations in photochemical control [20]; geomagnetic activity seasonal variations [6]; and variations in the meteorological activity [3,21,23,24]. Frissell et al. [24] concluded that there was no clear correlation between MSTID occurrence at midlatitude and space weather activity as parameterized by the indexes of geomagnetic activity AE and SYM-H. Rather, MSTID observations were found to have a correlation with the polar vortex dynamics with maximum MSTID occurrence during the periods of strong polar vortex [24]. Chernigovskaya et al. [26,27] also noted a possible relation of the winter enhancement in ionospheric variability with IGW sources in the underlying stratosphere.

Seasonal variations in the IGW structure in the upper mesosphere could be explained through the meridional-vertical circulation leading to adiabatic expansion and cooling of the mesopause in summer and to its compression and warming in winter [19]. Medvedev et al. [28] proposed that the probable cause for differences in the seasonal IGW variability of the atmosphere and of the ionosphere is the difference in the spatial and altitudinal location of the IGW sources.

In this study, we analyze a long series of short-period ionospheric TEC variability and mesopause temperature variability. For the first time, we perform a comparative joint analysis of IGW variability in different layers of the atmosphere and at different latitudinal sectors (from middle to high latitudes). We indicate a strong relation between the changes in the variability of the ionosphere, upper mesosphere, and high-latitude winter stratosphere, and examine this dependence at different latitudes.

2. Methodology

2.1. TEC Variability Analysis Method

For this study, we used the TEC data obtained from measurements by IGS GPS/GLONASS dual-frequency receivers [29] located in the mid-latitude (Irkutsk, 52.22°N, 104.32°E), subauroral (Yakutsk, 62.03°N, 129.68°E), and the high-latitude (Tiksi, 71.63°N, 128.87°E) regions. From phase and code measurements, we calculated series of vertical absolute TEC by the technique described in [30]; this technique enables to obtain long series of the vertical TEC values, considering differential code biases. We calculated the TEC series with a 15-min temporal resolution.

As a coefficient for short-term TEC variability we used *vrTEC* index, the *vrTEC* value is proportional to the TEC variation intensity within the range of periods T not exceeding the averaging period:

$$vrTEC(t) = \sqrt{\frac{\langle (TEC(t) - \langle TEC \rangle)^2 \rangle}{\langle TEC \rangle^2}} \cdot 100\% \quad (1)$$

where $\langle TEC \rangle$ is the TEC averaging over the time interval $t \pm 2$ hrs. Thus, the *vrTEC* reflects the level of short-term variability in the ionosphere. A similar approach was used in [19,26] that studied the seasonal dynamics of the IGW variation intensity in the data on the F2-layer electron density maximum. To analyze the seasonal dynamics of the intensity of TEC short-term variability, we averaged the obtained *vrTEC* values for a local day. As a result, one value for the mean variability level (*mvrTEC*) for each day was calculated.

2.2. Mesopause Temperature Variability Analysis Method

The mesopause region (80–100 km) is known to feature the lowest temperature values all year round, and its temperature regime experiences an active forcing from both solar radiation and wave processes originating in the low layers of the atmosphere [9]. To analyze the mesopause temperature regime, we used the data on the OH emission spectrometric observations at the observatories located near GNSS receivers.

To record the emission intensity at Tiksi (71.58° N, 128.77° E) and Maimaga (63.04°N, 129.51°E, near Yakutsk), we used photosensitive infra-red spectrographs within the 1490 - 1544 nm wavelength operation range. The detailed description of the instruments characteristics is in [31]. The spectrographs

measured the OH emission within the OH (3-1) band. At the Maimaga station, the spectrograph was assigned for continuous recording on 2013 January 17; at the high-latitude Tiksi station, it started continuous recording on 2015 September 3. The spectrographs record the OH (3-1) band in the near infra-red (about 1.5 μm), at $>9^\circ$ Sun immersion angle. The exposure time in order to obtain one measurement of the OH spectrum is 60 sec. The method to estimate the rotational temperature of the OH (3-1) molecular emissions is based on fitting model spectra for different temperatures (set in advance) to the actually measured spectrum [32]. When estimating the rotational temperature, we used the transition probabilities calculated in [33]. To exclude the high-noise data, we sampled the spectra meeting the >20 dB signal-to-noise ratio; then, we averaged the temperature at 3-min steps.

At the Tory observatory (51.80°N, 103.08°E, near Irkutsk), recording the OH spectra was performed by using a high-aperture diffraction spectrometer equipped by a high-sensitive digital receiver with a CCD-matrix. The detailed description of the instrument is presented in [34]. The spectra obtained with 10-minute temporal resolution are used to determine the spectral characteristics (intensity, temperature) of the hydroxyl molecule emission (band (6-2), 834.0 nm). The OH rotational temperature is calculated by the intensity distribution over the first three lines of the P1-branch of the vibration–rotation (6-2) band. Perminov et al. [35] described its determination method in detail.

The rotational temperature of a hydroxyl molecule reflects the atmospheric temperature at the emission maximum height (mesopause region). The indicated spectrographic methods enable to take the mesopause temperature at the $\sim 2^\circ\text{K}$ accuracy. The hydroxyl emitting layer intensity maximum is located at about 87 km, with the thickness of ~ 9 km [36]. In [37], the hydroxyl emission maximum height in the Meinel emission band is shown to differ by ~ 4 km. However, this difference is not essential in this study.

As a characteristic of the nightside wave activity, we accept the standard deviation of temperature T_i from its night-average value:

$$\sigma = \sqrt{\frac{1}{n} \sum (T_i - T)^2} \quad (2)$$

where n is the number of measured values within a night. The value for standard deviation σ includes intensities of various-period waves (tides, internal gravity waves) and the variations related to the dark current detector noise. We did not address planetary waves, because their timescale is much larger than one night. Therefore, the wave superposition may be presented like in [38]:

$$\sigma = \sqrt{\sigma_{td}^2 + \sigma_{gw}^2 + \sigma_{noise}^2} \quad (3)$$

where σ_{td} is the temperature variations caused by tidal waves, σ_{gw} is the temperature variations caused by internal gravity waves, σ_{noise} is the temperature standard deviation component caused by the dark current detector noise, which was calculated for each night of observations. The σ_{td} was determined by detecting the harmonics corresponding to the 24-, 12-, and 8-hr components of the diurnal tide from the nightside temperature series through the least square technique.

Equation (3) includes a component caused by the dark current detector noise (σ_{noise}). In Irkutsk, the dark current values were determined when the spectrometer entrance slit was closed, and the length of the measurement series was comparable with that of the hydroxyl emission observation series. The dark current relation to the hydroxyl emission intensity and temperature was empirically determined, and using this formula, the σ_{noise} values were calculated for every night of observation. In detail, the calculation procedure is described in [38,39].

Hence, knowing the σ_{td} and σ_{noise} , we calculated the contribution associated with the internal gravity wave activity σ_{gw} to the mesopause temperature variability. This technique was used in a number of papers [19,38–41] to analyze the mesopause temperature variability. As the measurements of the mesopause temperature in Tiksi/Yakutsk and in Irkutsk are based on different hydroxyl emission lines, its values may be related to slightly different heights of the mesosphere. However, in this work, we do not compare the temperature values themselves, but a short-period variability component in the

temperature. The extraction of σ_{gw} variations from the initial series of temperature T_i is carried out by the same technique. We believe that this allows us to compare properly the dynamics of the variability.

3. Results

3.1. Ionosphere Variability Dynamics

Figure 1a shows the variations in the indices of solar ($F_{10.7}$) and of geomagnetic (K_p) activities for 2002–2018. Panels b–d present the dynamics for the TEC variability mean coefficient ($mvrTEC$) at three stations (dark blue line displays the 27-day running mean reflecting the seasonal trend).

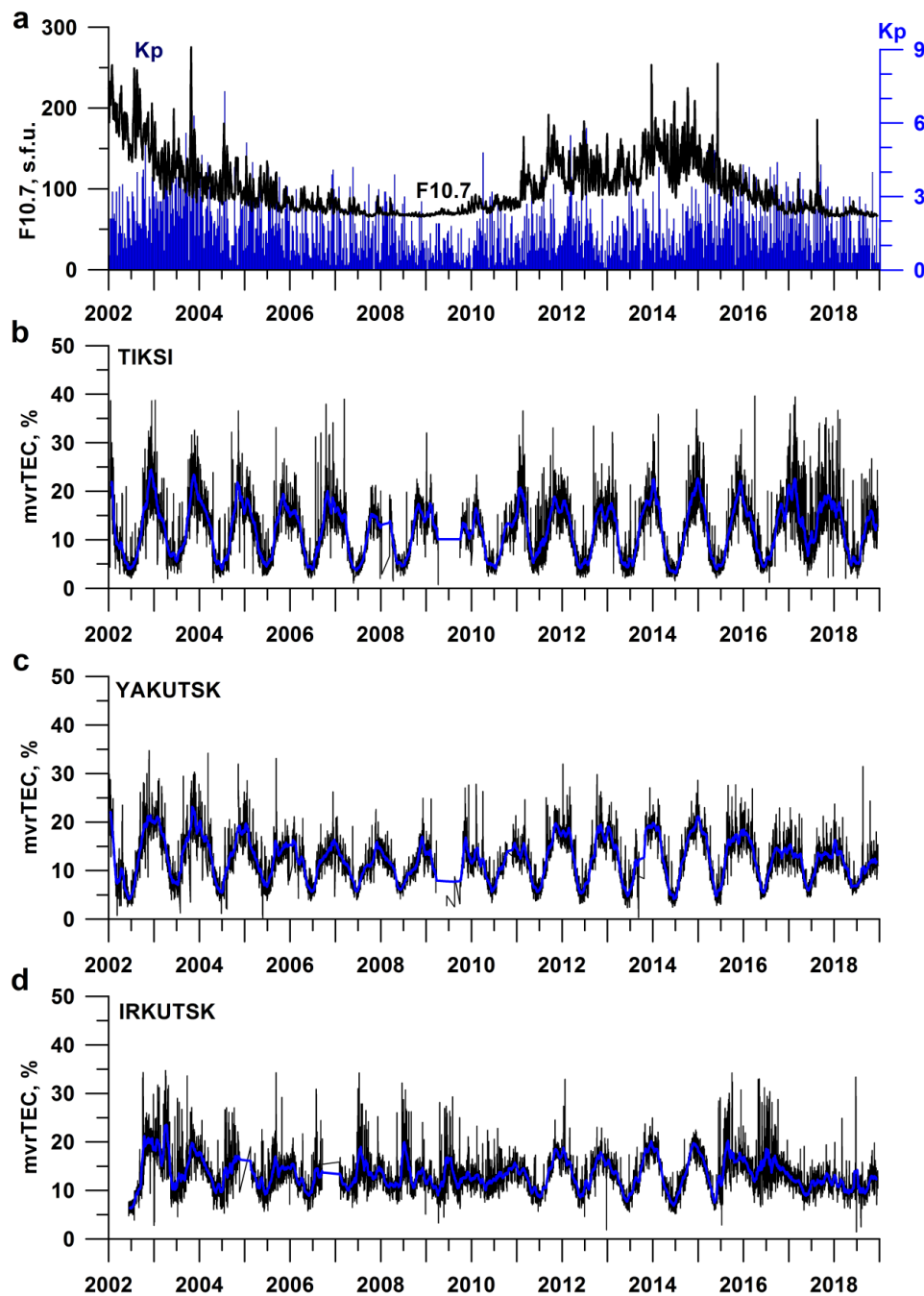


Figure 1. In the $F_{10.7}$ and K_p (a); $mvrTEC$ variations (black), and the 27-day running mean (dark blue) at Tiksi (b), Yakutsk (c), and Irkutsk (d) for 2002–2018.

Note that, in the short-term ionospheric disturbance dynamics, one does not observe any correlation with geomagnetic activity variation. This feature agrees with the results in [21,24]. In the TEC variability distributions, we trace a winter maxima dependence on solar activity. For example, at the Tiksi station, the disturbance maximum in winter months decreased from 25% in 2003 to about 15% in 2010 (i.e., the relative decrease is about 40%). A similar change is also observed at other stations. Interestingly, the variability level in summer months does not show a dependence on solar activity.

The *mvrTEC* values experience essential regular seasonal variations. Herewith, the seasonal variations are expressed more clearly at high-latitude stations and less explicitly are identified at mid-latitude Irkutsk. The least variability level at all the stations is recorded in summer months with the *mvrTEC* ~ 5% at Tiksi and Yakutsk, and ~ 10% at Irkutsk.

The *mvrTEC* peaks are recorded in winter periods, and they surpass by factor of 5-6 the disturbance level in the summer period. Herewith, in winter, the maximal values of the coefficient are observed at high-latitude Tiksi (~35-40%), while the minimal are recorded at mid-latitude Irkutsk (~ 20%). The difference between the winter and the summer values is also maximal at high latitudes. Individual bursts in the *mvrTEC* variations reflect individual major geomagnetic events.

Similar feature in the ionospheric disturbance seasonal variations was noted in the F2-layer electron density maximum behavior (N_mF2) from the DPS-4 ionosonde data for the solar activity minimum period [26]. Our results evidence that a similar seasonal variation in short-period ionospheric variability is characteristic, and it is observed at different levels of solar activity.

3.2. Upper Mesosphere Variability Dynamics

Figure 2 presents the variations reflecting the IGW activity in the gravity component σ_{gw} within the mesopause temperature data. The lines denote the running means with a 27-day averaging window, representing the seasonal variation in the gravity component σ_{gw} . Note that, due to the impossibility of the hydroxyl emission observations over the summer period (polar day), the data series in Tiksi and Maimaga have lacunae within summer months.

It is seen that IGW variability level in the upper mesosphere has the seasonal variation identical to that noted for the ionospheric disturbance. The coefficient σ_{gw} maximum is recorded in winter months (Dec-Jan-Feb), while the minimum is recorded in summer. At Tiksi and Maimaga, the temperature disturbance levels approximately coincide over the available observational seasons. The IGW component seasonal variation ranges 1.5°K through 6.5°K.

The seasonal variations in mesopause temperature variability in Irkutsk are expressed less significantly: the seasonal variation in the disturbance mean intensity changes ~3°K through ~4.5°K.

Note also a larger noisiness in the dynamic of variability in Irkutsk. Several factors may be the reason for the stronger noisiness in Irkutsk. The authors [38,39] studied variability of the mesopause temperature from the hydroxyl airglow OH (6-2) data obtained at two midlatitudinal sites, Zvenigorod and Irkutsk (Tory). At both observatories, measurements and data processing were performed using the same technique. The variability in temperature was calculated according to the same method as used in this work. A comparison of temperature variability revealed the enhanced values for Irkutsk compared to that obtained for Zvenigorod. This effect can be explained by the influence of the wave processes caused by the surrounding mountainous relief at Tory observatory on the mesopause temperature regime (orographical effect [42]). Tory station is located in the foothills of the Sayan Mountains. Another reason for the increased variability may be high seismic activity in the Baikal rift zone, where the Tory observatory is located. Thus, the influence of wave activity on the mesopause temperature regime for the Tory site can be more complicated compared to other sites. Additionally, the OH (3-1) transition is brighter than the OH (6-2) transition, which might lead to the smallest signal-to-noise ratio in data for Tory (Irkutsk) and, as a consequence, to greater noisiness in the data. Thus, we should bear in mind that the observed differences may be elucidated by not only different locations of the stations, although this factor is the most significant, but also by the different instruments employed for spectra recording.

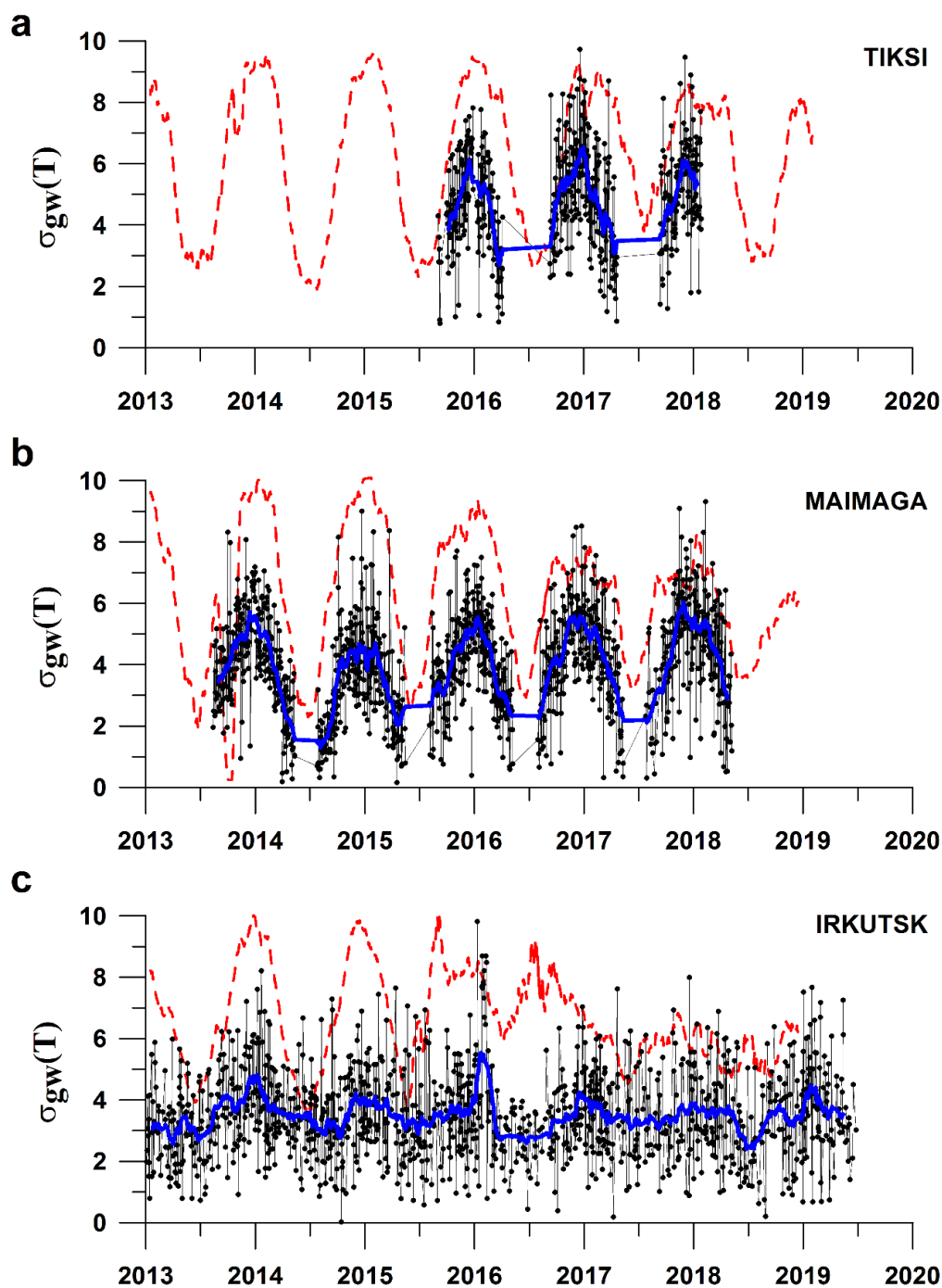


Figure 2. IGW component $\sigma_{gw}(T)$ variations within the mesopause temperature data (dots). The dark blue line superimposes the running mean with a 27-day window. Red dashed lines show the seasonal variations in TEC variability in half-scale of amplitude for corresponding regions.

4. Discussion

Essential seasonal variations observed regularly in the short-term variability of the ionosphere and of the upper mesosphere with the maximum in winter and with the minimum in summer do not correlate with the helio-geomagnetic variations. The sources for these variations may be processes occurring in the underlying atmosphere layers (stratosphere and troposphere).

The circumpolar vortex (CPV) and the CPV-related high-velocity jet stream (JS) is a source for IGW in the winter polar stratosphere and in the lower mesosphere [24,43–46]. The CPV represents a

cyclonic circulation large-scale cell that forms in a cold air mass over the polar region and encompasses the upper troposphere and the stratosphere. The CPV is accompanied by the evolution of a JS that is a narrow flow with the almost horizontal axis. The JS features large wind shears (both vertical and horizontal) and high velocity. Shpynev et al. [46] addressed the IGW generation mechanism in a high-velocity JS at stratospheric heights during the winter season. The authors showed that the vertical structure of the stratosphere wind in the JS features significant shear of the horizontal velocity, which facilitates inducing shear-layer instability. The instability appears as a source for gravity wave generation at the boundary surface. In [47], the authors detected and investigated the wave structures generated in a JS. They showed that the JS-carried full energy (per day) makes about 10^{17} J and, basically, it is generated at ~ 50 km in the stratopause. The bulk of this energy is spent on the flow radiation cooling. However, about 10–15% of the JS energy may be released for the IGW generation. Thereby, dynamic processes in a JS are one of the IGW basic sources in the winter middle atmosphere. Propagating upward, these waves transport the wave energy vertically into the mesosphere and into the lower thermosphere.

Figure 3 shows the distributions of the horizontal wind field (a, b) and of the atmospheric gas vertical velocity (c, d) at the stratopause level (1 hPa, about 52 km) on 2012 December 22 (a, c) and on 2013 January 6 (b, d), i.e., during the strong sudden stratosphere warming. Arrows on panels (a, b) show the direction of the air mass travel. The maps are built based on the ERA-Interim archive reanalysis data [48].

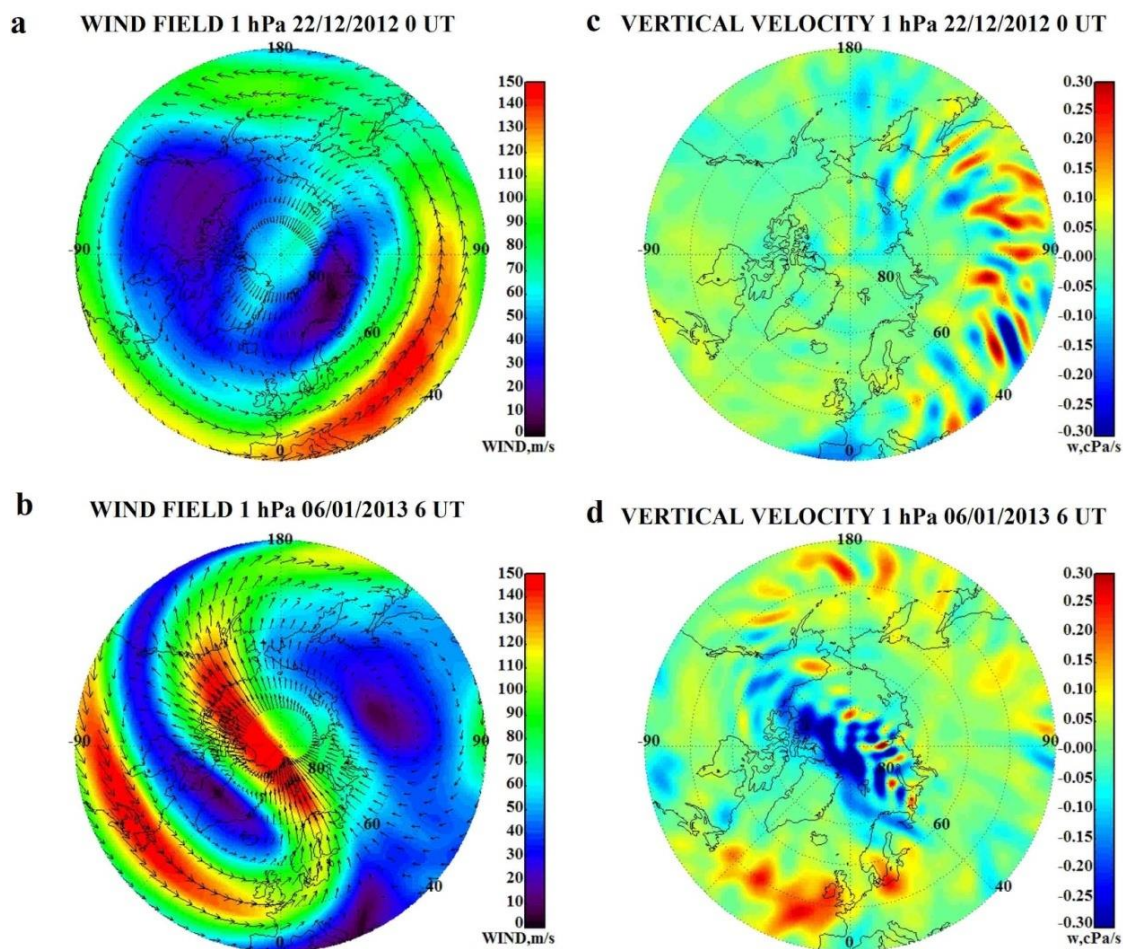


Figure 3. Horizontal wind field (a, b) and the atmospheric gas vertical velocity (c, d) at 1 hPa on 2012 December 22 (a, c) and on 2013 January 6 (b, d). Arrows on panels (a, b) show the direction of the air mass travel.

On the horizontal wind distributions, one can clearly distinguish a jet stream, the wind high velocity area surrounding the polar region. Wind velocities in a JS may reach 150 m/sec and higher. In quiet periods, a JS has a symmetric, almost ring-like structure (Figure 3a). During the sudden stratospheric warmings, there is an essential JS transformation and a displacement of its center from the pole (Figure 3b).

In the distributions of the atmospheric gas vertical velocity, one observes well-defined wave disturbances (Figure 3c,d). Herewith, the greatest intensity of such disturbances is recorded in the areas that coincide with the areas of the JS horizontal wind high velocities. Such wave disturbances are a feature of the winter polar stratosphere; they are related to stratospheric jet stream at 50–80°N [26]. The amplitude of these disturbances increases with height. Yasyukevich et al. [49] analyzed spatial spectra of the disturbances. The horizontal wavelength was revealed to vary within 300–3000 km, the vertical wavelength changed within 5–10 km, and the typical periods of the observed wave-like disturbances were estimated to be 50–250 minutes, i.e. IGW periods.

Based on the ERA-Interim data, we propose an index to estimate the level of the wave disturbance in the stratosphere (*stdW*). For this purpose, we calculated the standard deviation of the gas vertical velocity value from the zonal-mean value at the specified latitude in the mid stratosphere (10 hPa level) and at the stratopause (1 hPa).

Figure 4 presents the examples for latitude-temporal distributions of the *stdW* at 1 hPa and 10 hPa levels in 2009 and 2013. Apparently, an essential increase in the stratosphere disturbance level in both hemispheres is observed within a limited latitude range and has an expressed seasonal nature. The *stdW* maximal values are recorded during local winters in the subauroral regions (60–70°), where there is a well evolved polar vortex at that time and a high-velocity jet stream related to the latter.

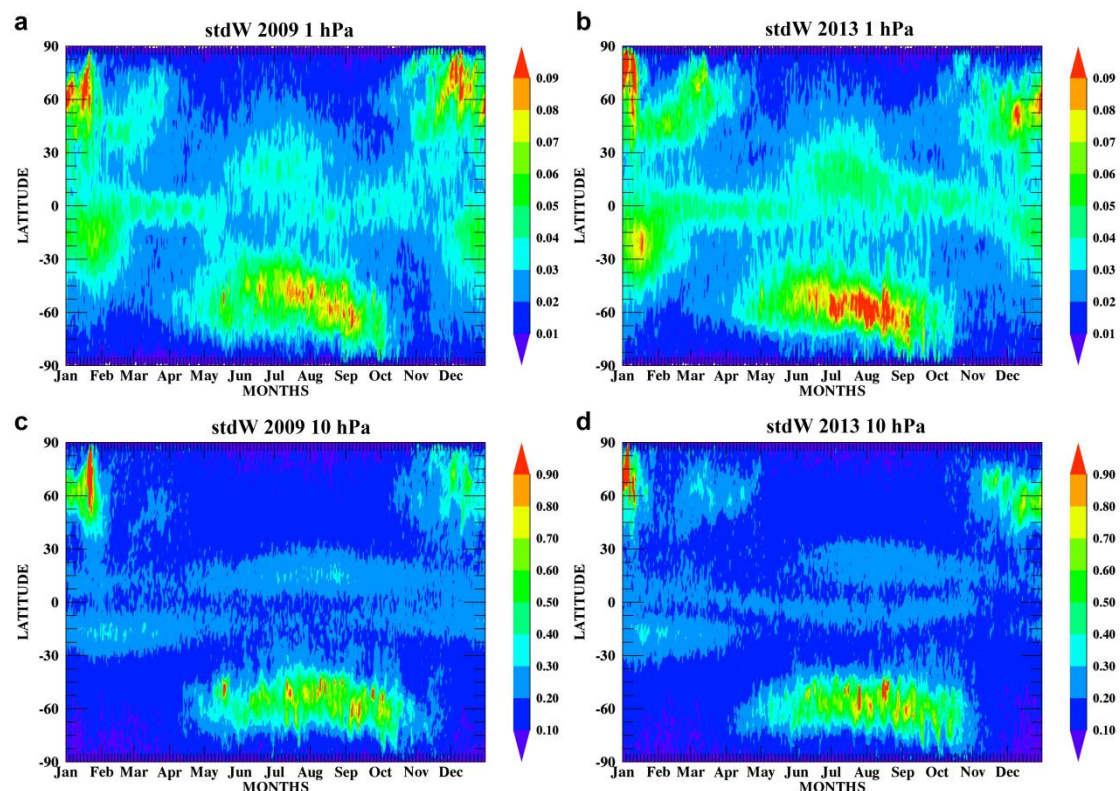


Figure 4. Latitude-temporal variations in the *stdW* at 1 hPa (a, b) and 10 hPa (c, d) in 2009 (a, c) and in 2013 (b, d). Latitudes are on the vertical scale, months of year are on the horizontal one.

Figure 5 shows the *stdW* long-term dynamics at 60°N in the mid and upper stratosphere. Apparently, the index values experience regular seasonal variations with the maximum in winter

months similar to those recorded for the ionospheric and mesospheric variability. The difference between the *stdW* summer and winter values is 5- or 6-fold. At that, unlike the disturbance in the ionosphere, there is no solar activity dependence traced for the stratosphere disturbance index.

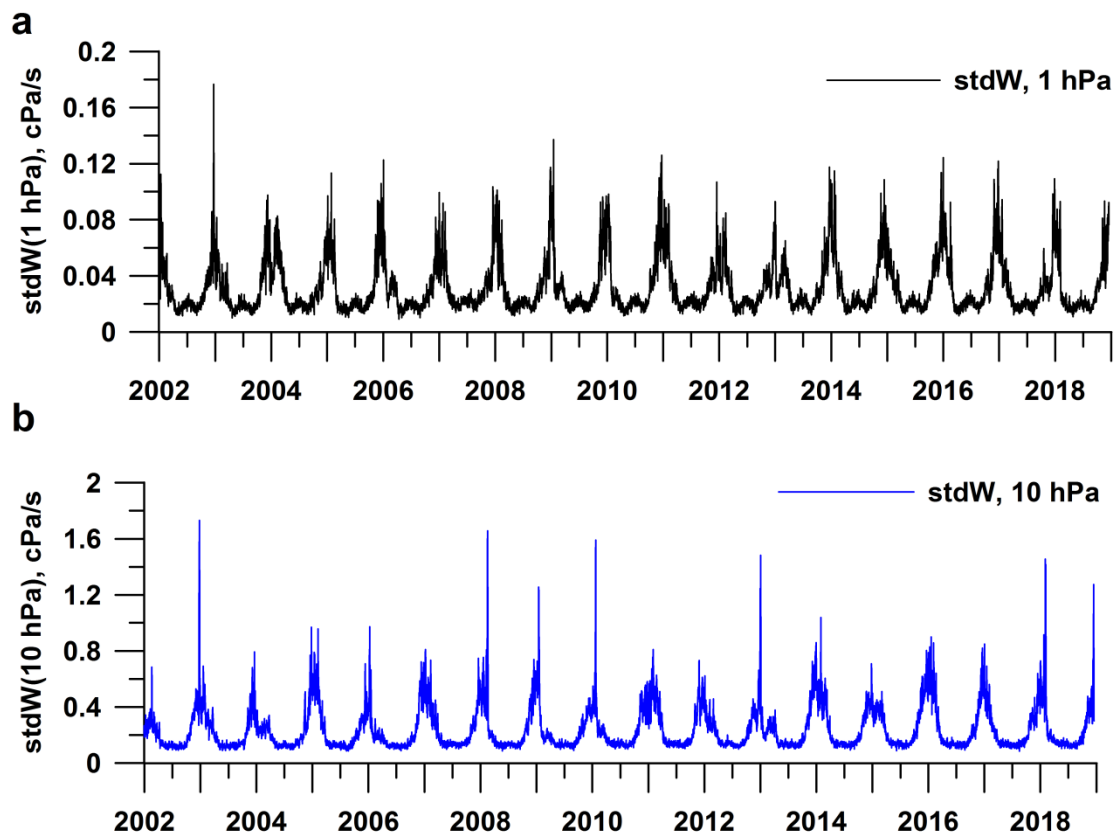


Figure 5. *StdW* variations at 60°N at 1 hPa (a, black) and 10 hPa (b, dark blue).

Figure 6 presents scatter-plots between the *stdW* at 1 hPa and the indices of the IGW disturbance in the mesosphere temperature $\sigma_{gw}(T)$ in Tiksi and Maimaga. Apparently, despite a noticeable scatter, one observes a sufficiently expressed dependence between these parameters. This dependence has a non-linear character. There, mesosphere disturbance saturation occurs, while the stratosphere disturbance intensity keeps growing. In the distributions, one also distinguishes the areas of the mesosphere disturbance increase in the absence of the stratosphere disturbance growth. The cause for these disturbances obviously is some other factors, i.e. solar and geomagnetic activity.

Figure 7 exhibits lagged cross-correlation functions for the short-term variability indexes between the stratosphere and mesosphere (a), and between the stratosphere and ionosphere (b) in Tiksi, Yakutsk (Maimaga), and Irkutsk. The positive lag values signify the time lag of the corresponding parameter from the stratosphere disturbance. Apparently, the correlation maximum for the mesosphere disturbance is ~ 0.65 in Irkutsk, 0.75 in Yakutsk, and exceeds 0.8 for high-latitude Tiksi. Note that the cross-correlation functions are sufficiently smooth sleek, and do not have an expressed maximum. However, one traces an increase in the lag of the correlation coefficient maximum with the latitude growth from 1 day in Irkutsk to more than 10 days in Tiksi.

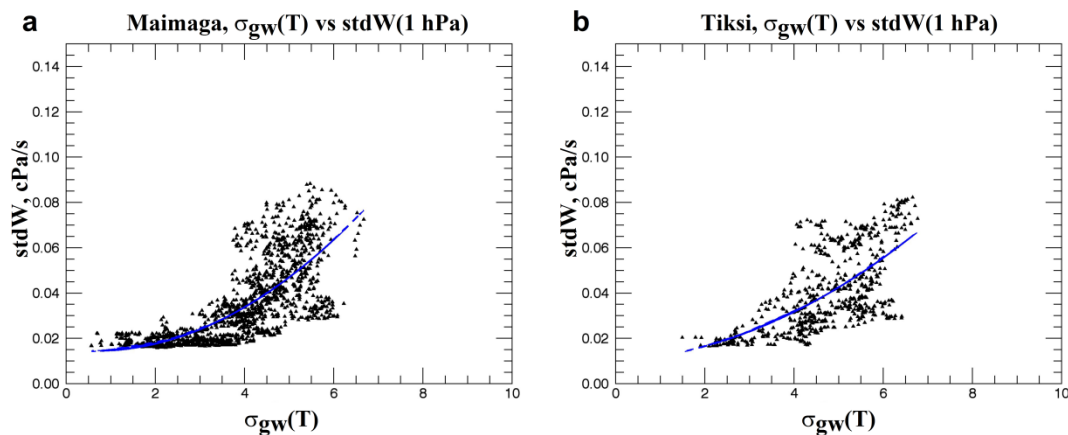


Figure 6. Scatter-plots between the variability indices in the stratosphere at 1 hPa and in the mesosphere at Maimaga (a) and Tiksi (b).

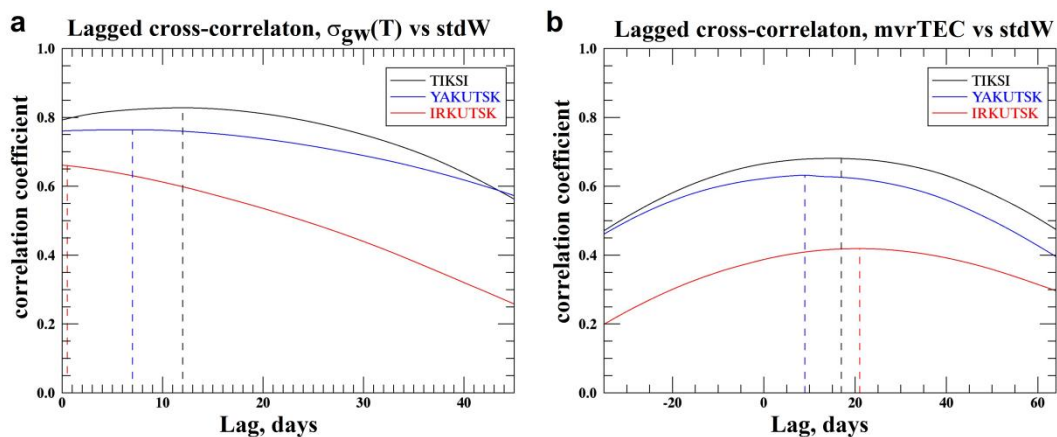


Figure 7. Lagged cross-correlation function between the variability indices in the stratosphere at 1 hPa and in the mesosphere (a), in the stratosphere and in the ionosphere (b) at Tiksi (black), Yakutsk (dark blue), and Irkutsk (red). Vertical dashed lines show the maxima of cross-correlation functions.

For the ionosphere disturbance, the correlation levels at all the stations are lower. The highest value for the correlation coefficient is recorded at Tiksi and makes near 0.7. The lowest value is observed in Irkutsk (only near 0.4). The cross-correlation function maximum at Tiksi and Yakutsk is observed with about a 10-day lag, while, in Irkutsk, the lag exceeds 25 days.

Thus, the correlation level with the stratosphere disturbance index is higher for the mesosphere disturbance, than that in the ionosphere. Both for the ionosphere and for the mesosphere variability, the correlation is substantially higher at high-latitude Tiksi. Supposedly, this is related to a closer location of the high-latitude points to the region, where the polar vortex exists. In the *mvrTEC* and in the σ_{gw} series obtained for Irkutsk, the seasonal variations were expressed most weakly, as well as a higher noise was observed here.

Lower correlation values for the ionosphere disturbance have a clear explanation. The ionosphere, besides the forcing from the lower neutral atmosphere, is subject to many disturbing factors, among which solar and geomagnetic activities prevail. All these factors contribute to the ionosphere disturbance level. However, one can trace a relation between the ionosphere short-term variability seasonal variations and the stratosphere disturbance fairly explicitly. In our opinion, the obtained results are a convincing demonstration of the interrelation between short-period variability in the ionosphere - upper mesosphere and the disturbances originating in the stratosphere polar vortex during winter months.

5. Conclusions

Based on the ionosphere TEC measurements and on the data of OH rotational temperature at the mesopause height, we have analyzed jointly the level of short-term variability at mid-latitude, subauroral, and high-latitude stations for a long time interval. The variability of chosen periods (up to several hours) is mostly related to IGWs activity in the upper atmosphere. The distributions of the short-term variability level, both in the ionosphere and at the mesopause height, are shown to experience similar regular seasonal variations. The variability maximum in the TEC and in the mesopause temperature is observed during winter months, and is 5- or 6-fold over the variability level during the summer period. This feature is observed every year for the period considered in this work. We have shown that the disturbance dynamics has no explicit relation to the levels of geomagnetic and solar activities.

We have suggested that a source of the recorded variations may be the processes occurring in the underlying atmospheric layers, specifically, in the high-velocity jet stream forming during winter months in the subauroral regions. The instabilities, evolving in the jet stream, are an IGW source. The IGWs propagating upward can cause disturbances of corresponding scales in the parameters of the upper atmosphere. We have proposed an index to estimate the stratosphere variability level. The stratosphere disturbance index is shown to experience similar regular seasonal variations with a maximum during winter months. We have shown a clear correlation between the mesosphere/ionosphere variability indices values and the stratosphere disturbance index. Furthermore, the correlation is higher for the mesosphere disturbance as compared with that in the ionosphere, and the correlation coefficient greatest values were recorded at the high-latitude station located closer to the region, where the disturbance generation occurs in the jet stream.

The obtained results indicate a strong interrelation between the short-period variability in the ionosphere, in the upper mesosphere, and in the subauroral stratosphere. Moreover, our results contribute to elucidating the basic mechanisms for a vertical coupling between different atmospheric layers.

Author Contributions: Conceptualization, A.Y. and M.C.; methodology, A.Y., I.M. and P.A.; investigation, A.Y., V.S. and I.M.; data curation, I.M., P.A. and G.G.; writing—original draft preparation, A.Y. and V.S.; writing—review and editing, A.Y. and I.M.; visualization, A.Y.; funding acquisition, A.Y. and I.M. All authors have read and agreed to the published version of the manuscript.

Funding: This study was funded by the Russian Science Foundation Grant No. 18-17-00042.

Acknowledgments: The authors are grateful to the IGS (<http://IGS.org/>) service for the data from navigation measurements, as well as to the ECMWF (<https://www.ecmwf.int/>) for the ERA Interim data. OH-emission data near Irkutsk were recorded by the Angara Multiaccess Center facilities at ISTP SB RAS (<http://ckp-angara.iszf.irk.ru/>) obtained with budgetary funding of Basic Research program II.16.

Conflicts of Interest: The authors declare no conflict of interest.

References

1. Hocke, K.; Schlegel, K. A review of atmospheric gravity waves and travelling ionospheric disturbances: 1982–1995. *Annal. Geophys.* **1996**, *14*, 917–940. [[CrossRef](#)]
2. Kazimirovsky, E.S. Coupling from below as a source of ionospheric variability: A review. *Ann. Geophys.* **2002**, *45*, 1–29. [[CrossRef](#)]
3. Lastovicka, J. Forcing of the ionosphere by waves from below. *J. Atmos. Sol. Terr. Phys.* **2006**, *68*, 479–497. [[CrossRef](#)]
4. Vadas, S.L. Horizontal and vertical propagation of gravity waves in thermosphere from lower atmospheric and thermospheric sources. *J. Geophys. Res.* **2007**, *112*, A06305. [[CrossRef](#)]
5. Fritts, D.C.; Alexander, M.J. Gravity wave dynamics and effects in the middle atmosphere. *Rev. Geophys.* **2003**, *41*, 1003. [[CrossRef](#)]
6. Rishbeth, H.; Mendillo, M. Patterns of F2-layer variability. *J. Atmos. Sol. Terr. Phys.* **2001**, *63*, 1661–1680. [[CrossRef](#)]

7. Forbes, J.M.; Palo, S.E.; Zhang, X. Variability of the ionosphere. *J. Atmos. Sol. Terr. Phys.* **2000**, *62*, 685–693. [[CrossRef](#)]
8. Liu, H.-L.; Yudin, V.A.; Roble, R.G. Day-to-day ionospheric variability due to lower atmosphere perturbations. *Geophys. Res. Lett.* **2013**, *40*, 665–670. [[CrossRef](#)]
9. Brasseur, G.; Solomon, S. *Aeronomy of the Middle Atmosphere: Chemistry and Physics of Stratosphere and Mesosphere*, 3rd ed.; Springer: Dordrecht, The Netherlands, 2005.
10. Noll, S.; Kausch, W.; Kimeswenger, S.; Unterguggenberger, S.; Jones, A.M. OH populations and temperatures from simultaneous spectroscopic observations of 25 bands. *Atmos. Chem. Phys.* **2015**, *15*, 3647–3669. [[CrossRef](#)]
11. Taylor, M.J.; Hapgood, M.A. On the origin of ripple-type wave structure in the OH nightglow emission. *Planet Space Sci.* **1990**, *38*, 1421–1430. [[CrossRef](#)]
12. Nakamura, T.; Higashikawa, A.; Tsuda, T.; Matsushita, Y. Seasonal variations of gravity wave structures in OH airglow with a CCD imager at Shigaraki. *Earth Planets Space* **1999**, *51*, 897–906. [[CrossRef](#)]
13. Vadas, S.L.; Taylor, M.J.; Pautet, P.-D.; Stamus, P.A.; Fritts, D.C.; Liu, H.-L.; São Sabbas, F.T.; Rampinelli, V.T.; Batista, P.; Takahashi, H. Convection: The likely source of the medium-scale gravity waves observed in the OH airglow layer near Brasilia, Brazil, during the SpreadFEx campaign. *Ann. Geophys.* **2009**, *27*, 231–259. [[CrossRef](#)]
14. Offermann, D.; Wintel, J.; Kalicinsky, C.; Knieling, P.; Koppmann, R.; Steinbrecht, W. Long-term development of short-period gravity waves in middle Europe. *J. Geophys. Res.* **2011**, *116*, D00P07. [[CrossRef](#)]
15. Gavrilov, N.M.; Manson, A.H.; Meek, C.E. Climatological monthly characteristics of middle atmosphere gravity waves (10 min–10 hr) during 1979–1993 at Saskatoon. *Ann. Geophys.* **1995**, *13*, 285–295. [[CrossRef](#)]
16. Gavrilov, N.M.; Fukao, S.; Nakamura, T.; Jacobi, C.; Kürschner, D.; Manson, A.H.; Meek, C.E. Comparative study of interannual changes of the mean winds and gravity wave activity in the middle atmosphere over Japan, Central Europe and Canada. *J. Atmos. Solar-Terr. Phys.* **2002**, *64*, 1003–1010. [[CrossRef](#)]
17. Popov, A.A.; Gavrilov, N.M.; Andreev, A.B.; Pogoreltsev, A.I. Interannual dynamics in intensity of mesoscale hydroxyl nightglow variations over Almaty. *Sol. Terr. Phys.* **2018**, *4*, 63–68. [[CrossRef](#)]
18. Taylor, M.J.; Pautet, P.-D.; Fritts, D.C.; Kaifler, B.; Smith, S.M.; Zhao, Y.; Criddle, N.R.; McLaughlin, P.; Pendleton, W.R.; McCarthy, M.P.; et al. Large-amplitude mountain waves in the mesosphere observed on 21 June 2014 during DEEPWAVE: 1. Wave development, scales, momentum fluxes, and environmental sensitivity. *J. Geophys. Res. Atmos.* **2019**, *10*, 364–384. [[CrossRef](#)]
19. Medvedeva, I.; Ratovsky, K. Studying atmospheric and ionospheric variabilities from long-term spectrometric and radio sounding measurements. *J. Geophys. Res. Space Phys.* **2015**, *120*, 5151–5159. [[CrossRef](#)]
20. Araujo-Pradere, E.A.; Fuller-Rowell, T.J.; Codrescu, M.V.; Bilitza, D. Characteristics of the ionospheric variability as a function of season latitude local time and geomagnetic activity. *Radio Sci.* **2005**, *40*, RS5009. [[CrossRef](#)]
21. Altadill, D. Time/altitude electron density variability above Ebro, Spain. *Adv. Space Res.* **2007**, *39*, 962–969. [[CrossRef](#)]
22. Ratovsky, K.G.; Medvedev, A.V.; Tolstikov, M.V. Diurnal, seasonal and solar activity pattern of ionospheric variability from Irkutsk Digisonde data. *Adv. Space Res.* **2015**, *55*, 2041–2047. [[CrossRef](#)]
23. Frissell, N.A.; Baker, J.B.H.; Ruohoniemi, J.M.; Gerrard, A.J.; Miller, E.S.; Marini, J.P.; West, M.L.; Bristow, W.A. Climatology of medium-scale traveling ionospheric disturbances observed by the midlatitude Blackstone SuperDARN radar. *J. Geophys. Res. Space Phys.* **2014**, *119*, 7679–7697. [[CrossRef](#)]
24. Frissell, N.A.; Baker, J.B.H.; Ruohoniemi, J.M.; Greenwald, R.A.; Gerrard, A.J.; Miller, E.S.; West, M.L. Sources and characteristics of medium-scale traveling ionospheric disturbances observed by high-frequency radars in the North American sector. *J. Geophys. Res. Space Phys.* **2016**, *121*, 3722–3739. [[CrossRef](#)]
25. Kotake, N.; Otsuka, Y.; Tsugawa, T.; Ogawa, T.; Saito, A. Climatological study of GPS total electron content variations caused by medium-scale traveling ionospheric disturbances. *J. Geophys. Res.* **2006**, *111*, A04306. [[CrossRef](#)]
26. Chernigovskaya, M.A.; Shpynev, B.G.; Ratovsky, K.G. Meteorological effects of ionospheric disturbances from vertical radio sounding data. *J. Atmos. Sol. Terr. Phys.* **2015**, *136*, 235–243. [[CrossRef](#)]

27. Chernigovskaya, M.A.; Shpynev, B.G.; Ratovsky, K.G.; Belinskaya, A.Y.; Stepanov, A.E.; Bychkov, V.V.; Grigorieva, S.A.; Panchenko, V.A.; Korenkova, N.A.; Mielich, J. Ionospheric response to winter stratosphere/lower mesosphere jet stream in the Northern Hemisphere as derived from vertical radio sounding data. *J. Atmos. Sol. Terr. Phys. J. Atmos. Sol. Terr. Phys.* **2018**, *180*, 126–136. [[CrossRef](#)]
28. Medvedev, A.V.; Ratovsky, K.G.; Tolstikov, M.V.; Alsatkin, S.S.; Scherbakov, A.A. Studying of the spatial–temporal structure of wavelike ionospheric disturbances on the base of Irkutsk incoherent scatter radar and digisonde data. *J. Atmos. Sol. Terr. Phys.* **2013**, *105*, 350–357. [[CrossRef](#)]
29. Dow, J.M.; Neilan, R.E.; Rizos, C. The International GNSS Service in a changing landscape of Global Navigation Satellite Systems. *J. Geod.* **2009**, *83*, 191–198. [[CrossRef](#)]
30. Yasyukevich, Y.V.; Mylnikova, A.A.; Polyakova, A.S. Estimating the total electron content absolute value from the GPS/GLONASS data. *Res. Phys.* **2015**, *5*, 32–33. [[CrossRef](#)]
31. Sivtseva, V.I.; Ammosov, P.P.; Gavriilyeva, G.A.; Koltovskoi, I.I.; Ammosova, A.M. Comparison between seasonal variations in tidal and internal gravity wave activity as derived from observations at Maimaga and Tiksi. *Solar Terr. Phys.* **2018**, *4*, 69–72. [[CrossRef](#)]
32. Ammosov, P.P.; Gavriilyeva, G.A. Infrared Digital Spectrograph for Measuring Hydroxyl Rotational Temperature. *Instrum. Exp. Tech.* **2000**, *43*, 792–797. [[CrossRef](#)]
33. Mies, F.H. Calculated Vibrational Transition Probabilities of OH(X²Π). *J. Mol. Spectrosc.* **1974**, *53*, 150–180. [[CrossRef](#)]
34. Semenov, A.I.; Bakanas, V.V.; Perminov, V.I.; Zheleznov, Y.A.; Khomich, V.Y. The near infrared spectrum of the emission of the nighttime upper atmosphere of the Earth. *Geomagnetism Aeronomy* **2002**, *42*, 390–397.
35. Perminov, V.I.; Semenov, A.I.; Shefov, N.N. On rotational temperature of the hydroxyl emission. *Geomagnetism Aeronomy* **2007**, *47*, 756–763. [[CrossRef](#)]
36. Baker, D.J.; Stair, A.T. Rocket measurements of the altitude distributions of the hydroxyl airglow. *Phys. Scripta* **1988**, *37*, 611–622. [[CrossRef](#)]
37. Von Savigny, C.; McDade, I.C.; Eichmann, K.-U.; Burrows, J.P. On the dependence of the OHMeinel emission altitude on vibrational level: SCIAMACHY observations and model simulations. *Atmos. Chem. Phys.* **2012**, *12*, 8813–8828. [[CrossRef](#)]
38. Perminov, V.I.; Semenov, A.I.; Medvedeva, I.V.; Pertsev, N.N. Temperature Variations in the Mesopause Region According to the Hydroxyl-Emission Observations at Midlatitudes. *Geomagnetism Aeronomy* **2014**, *54*, 230–240. [[CrossRef](#)]
39. Perminov, V.I.; Semenov, A.I.; Medvedeva, I.V.; Zheleznov, Y.A. Variability of mesopause temperature from the hydroxyl airglow observations over midlatitudinal sites, Zvenigorod and Tory, Russia. *Adv. Space Res.* **2014**, *54*, 2511–2517. [[CrossRef](#)]
40. Bittner, M.; Offermann, D.; Graef, H.-H.; Donner, M.; Hamilton, K. An 18-year time series of OH rotational temperatures and middle atmosphere decadal variations. *J. Atmos. Sol. -Terr. Phys.* **2002**, *64*, 1147–1166. [[CrossRef](#)]
41. Offermann, D.; Gusev, O.; Donner, M.; Forbes, J.M.; Hagan, M.; Mlynczak, M.G.; Oberheide, J.; Preusse, P.; Schmidt, H.; Russell, J.M., III. Relative intensities of middle atmosphere waves. *J. Geophys. Res.* **2009**, *114*, D06110. [[CrossRef](#)]
42. Chunchuzov, I.P. On possible generation mechanism for nonstationary mountain waves in the atmosphere. *J. Atmos. Sci.* **1994**, *15*, 2196–2206. [[CrossRef](#)]
43. Wu, D.L.; Waters, J.W. Satellite observations of atmospheric variances: A possible indication of gravity waves. *Geophys. Res. Lett.* **1996**, *23*, 3631–3634. [[CrossRef](#)]
44. Whiteway, J.A.; Duck, T.J.; Donovan, D.P.; Bird, J.C.; Pal, S.R.; Carswell, A.I. Measurements of gravity wave activity within and around the Arctic stratospheric vortex. *Geophys. Res. Lett.* **1997**, *24*, 1387–1390. [[CrossRef](#)]
45. Gerrard, A.J.; Bhattacharya, Y.; Thayer, J.P. Observations of in-situ generated gravity waves during a stratospheric temperature enhancement (STE) event. *Atmos. Chem. Phys.* **2011**, *11*, 11913–11917. [[CrossRef](#)]
46. Shpynev, B.G.; Churilov, S.M.; Chernigovskaya, M.A. Generation of waves by jet-stream instabilities in winter polar stratosphere/mesosphere. *J. Atmos. Sol. -Terr. Phys.* **2015**, *136*, 201–215. [[CrossRef](#)]
47. Shpynev, B.G.; Khabituev, D.S.; Chernigovskaya, M.A.; Zorkal'tseva, O.S. Role of winter jet stream in the middle atmosphere energy balance. *J. Atmos. Sol. Terr. Phys.* **2019**, *188*, 1–10. [[CrossRef](#)]

48. Dee, D.P.; Uppala, S.M.; Simmons, A.J.; Berrisford, P.; Poli, P.; Kobayashi, S.; Andrae, U.; Balmaseda, M.A.; Balsamo, G.; Bauer, P.; et al. The ERA-Interim reanalysis: Configuration and performance of the data assimilation system. *Q. J. R. Meteorol. Soc.* **2011**, *137*, 553–597. [[CrossRef](#)]
49. Yasyukevich, A.S.; Chernigovskaya, M.A.; Mylnikova, A.A.; Shpynev, B.G.; Khabituev, D.S. Seasonal and helio-geomagnetic activity pattern of the ionospheric variability over Russia’s Eastern Siberia and Far East region from the GPS/GLONASS data. In Proceedings of the 2017 Progress in Electromagnetics Research Symposium—Spring (PIERS), St. Petersburg, Russia, 22–25 May 2017; pp. 2015–2022. [[CrossRef](#)]



© 2020 by the authors. Licensee MDPI, Basel, Switzerland. This article is an open access article distributed under the terms and conditions of the Creative Commons Attribution (CC BY) license (<http://creativecommons.org/licenses/by/4.0/>).